crystals

MDPI

Article

Properties of $LiGa_{0.5}In_{0.5}Se_2$: A Quaternary Chalcogenide Crystal for Nonlinear Optical Applications in the Mid-IR

Ludmila Isaenko [1,2], Alexander Yelisseyev [1], Sergei Lobanov [1], Vitaliy Vedenyapin [1], Pavel Krinitsyn [1] and Valentin Petrov [3,*]

1 Laboratory of Crystal Growth, Institute of Geology and Mineralogy, SB RAS, 3 Ac. Koptyuga Ave., 630090 Novosibirsk, Russia; lyudmila.isaenko@mail.ru (L.I.); elissev.ap@mail.ru (A.Y.); singlecrystal@ngs.ru (S.L.); blackraven@ngs.ru (V.V.); sagwerbs@yandex.ru (P.K.)

2 Laboratory of Semiconductor and Dielectric Materials, Novosibirsk State University, 2 Pirogova Str., 630090 Novosibirsk, Russia

3 Max-Born-Institute for Nonlinear Optics and Ultrafast Spectroscopy, 2A Max-Born-Str., D-12489 Berlin, Germany

* Correspondence: petrov@mbi-berlin.de; Tel.: +49-30-6392-1272

Academic Editor: Ning Ye

Received: 22 June 2016; Accepted: 22 July 2016; Published: 28 July 2016

Abstract: $LiGaSe_2$ (LGSe) and $LiInSe_2$ (LISe) are wide band-gap nonlinear crystals transparent in the mid-IR spectral range. $LiGa_{0.5}In_{0.5}Se_2$ (LGISe) is a new mixed crystal, a solid solution in the system LGSe–LISe, which exhibits the same orthorhombic structure (*mm*2) as the parent compounds in the same time being more technological with regard to the growth process. In comparison with LGSe and LISe its homogeneity range is broader in the phase diagram. About 10% of the Li ions in LGISe occupy octahedral positions (octapores) with coordination number of 3. The band-gap of LGISe is estimated to be 2.94 eV at room temperature and 3.04 eV at 80 K. The transparency at the 0-level extends from 0.47 to 13 μm. LGISe crystals exhibit luminescence in broad bands centered near 1.7 and 1.25 eV which is excited most effectively by band-to-band transition. From the measured principal refractive indices and the fitted Sellmeier equations second-harmonic generation from 1.75 to 11.8 μm (fundamental wavelength) is predicted. The nonlinear coefficients of LGISe have values between those of LGSe and LISe. ^{6}LGISe crystals are considered promising also for detection of thermal neutrons.

Keywords: nonlinear optical crystals; ternary and quaternary chalcogenides; solid solution; mid-IR

1. Introduction

The orthorhombic lithium ternary chalcogenides with the chemical formula $LiBC_2$ where B=In and Ga, C=S and Se, occupy a special position among the non-oxide nonlinear optical crystals because they are characterized by the widest band-gaps [1–7]. Thus, their main advantage consists in the possibility to pump them at rather short wavelengths (in the near-IR), without two-photon absorption (TPA), generating tunable mid-IR radiation by frequency down-conversion nonlinear optical processes [8]. The wider band-gap, in comparison e.g., to their chalcopyrite type $AgBC_2$ analogues, also leads to increased damage threshold and relatively weak refractive index dispersion in the infrared which is important for frequency conversion of short laser pulses. In addition, the thermal conductivity of the four $LiBC_2$ compounds is also higher compared to their $AgBC_2$ counterparts, which is an essential advantage at high average powers. Whereas the chalcopyrites $AgBC_2$ exhibit strong anisotropy of the thermal extension with opposite sign of the coefficients along different crystallographic directions (parallel and perpendicular to the optical axis *c*), these coefficients show only slight anisotropy in the

$LiBC_2$ compounds. The latter makes it possible to select any desirable orientation for the seed in the process of crystal growth.

In the chalcopyrite family of nonlinear crystals $AgBC_2$, all four types of solid solutions have been studied but in the limit of $AgInC_2$, the birefringence is too low for phase-matching. Ternary sulfides and selenides with the general formula $AgBC_2$ and chalcopyrite structure readily form continuous series of isovalent substitutional solid solutions and this is true in particular for the $AgGaSe_2$–$AgInSe_2$ system [9–11]. Mixed crystals of $AgGa_{1-x}In_xSe_2$ with In content up to 42% were grown [9] and it was shown that $AgGa_{1-x}In_xSe_2$ nonlinear crystals possess considerable potential for the realization of noncritically phase-matched three-photon interactions [9,11]. In contrast to the $AgInC_2$ family, all four wurtzite type $LiBC_2$ compounds possess sufficient birefringence and obviously all their properties can be continuously tuned by engineering the composition. The growth of two such solid solutions, $LiIn(S_{1-x}Se_x)_2$ [12] and $LiGa_{1-x}In_xSe_2$ [13], has been reported for $x = 0.5$. The present work is devoted to the characterization of $LiGa_{0.5}In_{0.5}Se_2$ (LGISe).

Crystal engineering in the system $LiGaSe_2$ (LGSe)−$LiInSe_2$ (LISe) is potentially interesting because although most of the properties of the two parent compounds are quite similar and interpolation is expected to provide a reliable estimate of the expected characteristics, the difference for a given three-wave interaction process pumped by a specific laser system can be rather large. Thus, e.g., amplified Ti:sapphire laser systems, the most advanced sources of high energy femtosecond pulses, can be used for pumping parametric amplifiers based on LGSe but not LISe although the latter exhibits the highest nonlinearity among the $LiBC_2$ compounds. This limitation is a consequence of the different band-gaps: as a result of this the TPA coefficient measured at 820 nm is <0.07 cm/GW for LGSe but as large as 0.6 cm/GW for LISe [2].

The situation is similar in another important application of the Li-containing chalcogenides, namely for detection of thermal neutrons, where also a trade-off of properties is required. This application is based on the high thermal neutron cross section (938 barns) of the ^6Li isotope which converts thermal neutrons to highly ionizing particles through the nuclear reaction $^6Li(n,\alpha)^3H$, while the $LiBC_2$ semiconductors detect the electron-hole pairs induced by either tritium ions or α-particles [14]. Among the $LiBC_2$ crystals maximum response has been demonstrated with LISe which exhibits the minimum band-gap. On the other hand, thermal neutrons can be detected by recording the light pulses generated as a result of the interaction of the crystal with ionizing particles: in this case LISe operates as a scintillator [15]. The problem is the natural abundance of ^6Li which amounts to only 7.5%. To increase the detection efficiency LISe crystals with lithium as ^6Li can be grown [16]. However, ^{115}In (with natural abundance of 95.7%) present in LISe also captures neutrons, which results in gamma decay rather than charge creation. From this point of view, replacing In- by Ga-ions can potentially increase the efficiency of the neutron detection [17]. Compositions with 25%, 50%, and 85% substitution were grown in [17].

The present paper presents information on the growth procedure, crystal structure, and the linear and nonlinear optical properties (including photoluminescence, dispersion of refractive indices, phase-matching conditions) of LGISe.

2. Crystal Growth and Structure

LGISe was obtained from the two compounds LISe and LGSe, taken in stoichiometric ratio. The two ternary lithium selenides were first synthesized by the methodology described in previous work [3,5]. The melting temperature of the quaternary LGISe is lower (830 °C) than the melting temperatures of both LISe (905 °C) and LGSe (915 °C). The synthesis of the quaternary compound was carried out in a glass graphite crucible located inside a silica container, for 4 h at T = 970 °C in Ar atmosphere. The obtained charge of the quaternary compound was backfilled into a glass graphite crucible. A conical bottom of the crucible provides a separation of the single crystal nucleus during the growth process. The crucible was then inserted into a silica ampoule. The ampoule was evacuated to 10^{-3} Pa, then filled with dry Ar to provide some overpressure (about 1000 Pa) and finally sealed.

In [18] the process of incongruent evaporation was studied in detail for both LISe and LGSe compounds at temperatures near the melting point. The perfection of a bulk crystal of certain composition depends on the growth conditions such as the maximum temperature and the time of melt overheating. According to our data, an overheating exceeding 50 °C results in strong shift of the compound composition away from the stoichiometric one. Volatile components with a high partial pressure of $Ga(In)_2Se_3$ escape from the reaction area and migrate into the free area of the reactor. Ar overpressure in the reactor solves partly the problem. The lower synthesis and growth temperatures of LGISe suppress the effect of incongruent sublimation and thus from the point of view of crystal growth, the quaternary compound seems quite promising for achieving good optical quality.

The growth of LGISe single crystals was carried out by a modified vertical Bridgman-Stockbarger technique. The ampoule was quiescently located in the furnace, in a position with temperature gradient of 15 to 30 °C/cm. The furnace was heated at a rate of 100 °C/h to a temperature exceeding the melting point by 50 °C. This temperature was maintained for 10 h and then the furnace was slowly cooled down following a program which ensured a crystal growth rate of 0.1 to 1.0 mm/day during the entire growth process. Finally, the furnace was switched-off. The as-grown crystals had a diameter of 20 mm and a length of up to 50 mm but were milky (Figure 1a). This required additional annealing in vacuum or in Se vapor at 750 °C for a period of 3 h to obtain high transparency. The resulting color varied from yellow to pink depending on the deviation from stoichiometry. In Figure 1b, two semiprisms of LGISe are shown in transmitted light: they were used to study the dispersion of the refractive indices and the birefringence. The annealed LGISe crystals show a dark red luminescence under UV excitation at 365 nm (Figure 1c).

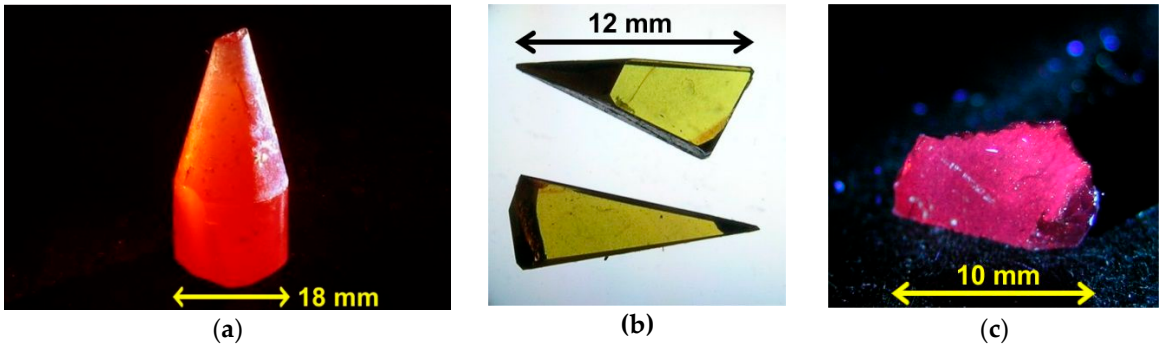

(**a**) (**b**) (**c**)

Figure 1. (**a**) As-grown LGISe boule; (**b**) LGISe semiprisms in transmitted light; (**c**) Photoluminescence (PL) pattern of annealed LGISe under UV excitation.

The crystal structure of LGISe was studied on single crystals with Oxford Diffraction Gemini R Ultra (Oxford Diffraction Ltd., Abingdon, UK) and Bruker P4 (Bruker Advanced X-Ray Solutions, Madison, WI, USA), MoKα λ = 0.71073 Å diffractometers, using the SHELXL-97 program (George Sheldrick, Göttingen, Germany). The LGISe structure is similar to that of the two parent ternary compounds: β-$NaFeO_2$ structure with space group $Pna2_1$ or C_{2v}^9 (Table 1). The structure of the orthorhombic (point group *mm*2) $LiBSe_2$ compounds is formed by $LiSe_4$ and BSe_4 tetrahedrons, and the Se-ions are arranged in hexagonal packing with tetragonal and octahedral cavities (tetrapores and octapores). Only half of the tetrapores are normally occupied by Li- and B-ions while all octapores are normally empty. The structure of the parent components LISe and LGSe exhibits some characteristic features. Li ions occupy two nonequivalent sites (in tetra- and octapores) in LISe but there is only one such site (in tetrapores) in LGSe. The structure of the mixed LGISe crystal inherits this feature from the LISe component: about 10% of the Li ions occupy octapores (Tables 2 and 3, Figure 2). Thus, the LGISe structure is considered to contain the two subsystems. The unit cell parameters of LGISe are a = 7.0376(2) Å, b = 8.3401(3) Å, and c = 6.6855(2) Å. The unit cell volume is 392.4 $Å^3$, larger compared to LGSe and smaller compared to LISe. The composition of the bulk crystals was determined by a

high-accuracy chemical analysis, and the phase state was controlled by X-ray diffraction. Assuming linear change of the lattice parameters with composition of the $LiGa_xIn_{1-x}Se_2$ solid solutions, the experimentally measured lattice parameters would correspond to a composition with x = 0.42–0.43.

Table 1. Crystal data and structure refinement details for $LiGa_{0.5}In_{0.5}Se_2$.

Formula	$\mathbf{LiGa_{0.5}In_{0.5}Se_2}$
formula weight (g/mol)	257.13
crystal system	orthorhombic
space group	$Pna2_1$
unit cell dimensions (Å)	a = 7.0376(2), b = 8.3401(3), c = 6.6855(2)
V (Å^3); Z	392.40(2)/4
calculated density (g/cm^3)	4.352
crystal size (mm)	0.1 × 0.2 × 0.2
μ (MoKα) (mm^{-1})	24.809
θ range (deg) for data collection	3.79–32.57
Miller index ranges	$-10 \leqslant h \leqslant 10$, $-12 \leqslant k \leqslant 11$, $-5 \leqslant l \leqslant 10$
reflections collected/unique	3883/1213 (R(int) = 0.0250)
data/restraints/parameters	1213/1/39
goodness-of-fit on F^2 (GOF)	0.663
final R indices ($I > 2\sigma(I)$)	$R(F)$ = 0.0129, $wR(F^2)$ = 0.0486
R indices (all data)	$R(F)$ = 0.0183, $wR(F^2)$ = 0.0594
absolute structure parameter	0.040(19)
extinction coefficient	0.0107(8)
largest difference peak/hole (e·Å^{-3})	0.338/−0.424

Table 2. Atomic coordinates and equivalent isotropic atomic displacement parameters for $LiGa_{0.5}In_{0.5}Se_2$.

Atom	*x*/*a*	*y*/*b*	*z*/*c*	U_{eq} (Å^2)
In/Ga *	0.57623(3)	0.62606(2)	0.38637(16)	0.0157(1)
Se(1)	0.41137(5)	0.87170(4)	0.50826(6)	0.0207(2)
Se(2)	0.57352(4)	0.62421(4)	0.01222(8)	0.0204(2)
Li(1) **	0.5841(10)	0.1209(7)	0.378(4)	0.024(3)
Li(2) ***	0.257(10)	0.114(6)	0.142(11)	0.03(3)

* refined site occupancy factor (sof): 0.52(1)/0.48(1) for In/Ga, respectively; ** sof: 0.90(5); *** sof: 0.10(5).

Table 3. Selected interatomic distances (Å) in $LiGa_{0.5}In_{0.5}Se_2$.

In-Tetrahedron	Li(1)-Tetrahedron	Li(2)-Pyramid
In–Se(2 [a]) 2.4850(6)	Li(1)–Se(2 [a]) 2.56(1)	Li(2)–Se(1 [c]) 2.50(7)
In–Se(1) 2.4915(5)	Li(1)–Se(1 [c]) 2.47(3)	Li(2)–Se(1 [f]) 2.52(6)
In–Se(1 [b]) 2.4954(5)	Li(1)–Se(2 [d]) 2.57(1)	Li(2)–Se(2 [g]) 2.61(6)
In–Se(2) 2.5015(13)	Li(1)–Se(1[e]) 2.56(1)	-
<In–Se> 2.4934	<Li(1)–Se> 2.54	<Li(2)–Se> 2.54

Symmetry codes: [a] $-x+1, -y+1, z+1/2$; [b] $x+1/2, -y+3/2, z$; [c] $-x+1, -y+1, z-1/2, -z+1$; [d] $-x+3/2, y-1/2, z+1/2$; [e] $x, y-1, z$; [f] $x-1/2, -y+1/2, z$; [g] $-x+1/2, y-1/2, z$.

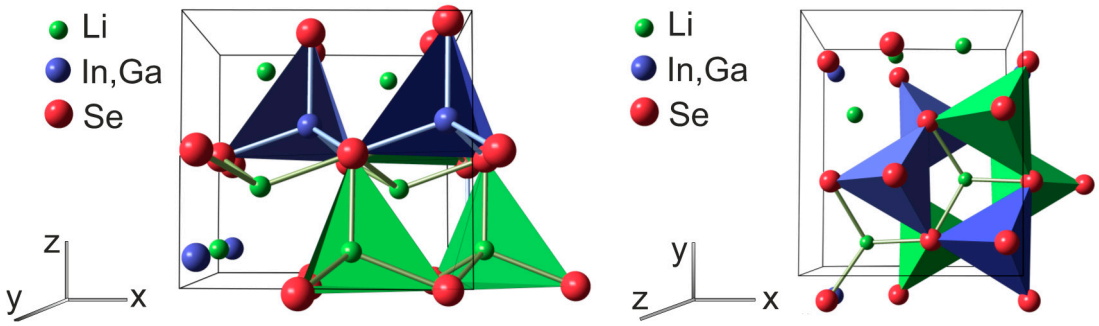

Figure 2. $LiGa_{0.5}In_{0.5}Se_2$ possesses the same β-$NaFeO_2$-type structure as the four ternary $LiBC_2$ compounds. At room temperature and normal pressure the major part of the Li ions occupy tetrapores in the LGISe structure and only about 10% of the Li ions are localized inside octapores.

3. Transmission and Luminescence

The transmission of the as-grown yellow LGISe crystals was measured using a conventional spectrophotometer in the UV to near-IR and a Fourier-transform spectrophotometer in the mid-IR, Figure 3. It extends roughly from 0.47 to 13.5 μm at the 0-level for 7 mm thick LGISe samples. Thus, LGISe can be pumped at 1064 nm without TPA. Variations of LGISe color from yellow to pink are possible: the corresponding transmission spectra are given in Figure 3. Yellow and pink crystals have similar transmission spectra with broad absorption bands around 2.6 and 10.3 μm in the infrared. In the visible region there is a broad band around 0.6 μm. In pink samples the fundamental absorption edge shifts to 0.515 μm and an additional absorption feature appears in the 0.6–0.8 μm range. For thin LGISe plates of light yellow color, the fundamental absorption edge shifts to 0.42 μm at 300 K and to 0.395 μm at 80 K (Figure 3).

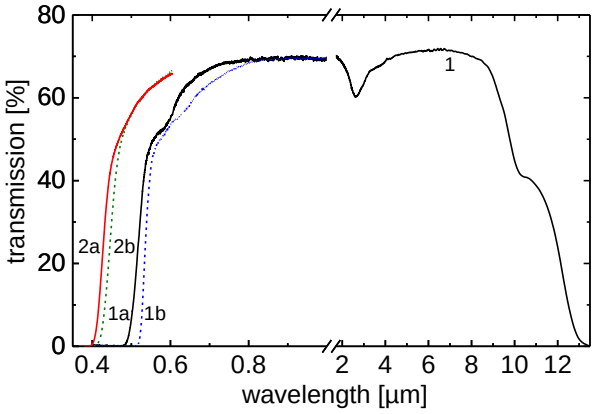

Figure 3. Unpolarized transmisson spectra of $LiGa_{0.5}In_{0.5}Se_2$ crystals, 7 mm (1) and 60 μm (2) thick. Fragments 1a and 1b were recorded at 300 K in areas of yellow and pink color, respectively. Fragments 2a and 2b were recorded for a 60 μm thick light yellow plate at 80 and 300 K, respectively.

The band-gap was estimated from measurements of the absorption coefficient α with a 60 μm thin plate of LGISe, Figure 4. From linear fits of the $(\alpha h\nu)^2$ dependence on $h\nu$ (the case of direct allowed transitions between parabolic bands) one arrives at 2.94 eV at 300 K which corresponds to 0.42 μm. At 80 K, the band-gap E_g is 3.04 eV. For comparison, the band-gaps of LGSe and LISe are 3.34 and 2.86 eV, respectively [1,6]. It is necessary to note that the E_g value for LGISe is closer to LISe than to LGSe. This means that the electric conductivity of LGISe should be closer to that of LISe and as a result their response to thermal neutrons should be similar. Moreover, as mentioned before, substituting roughly half of the In-ions by Ga-ions improves the efficiency of the neutron detection.

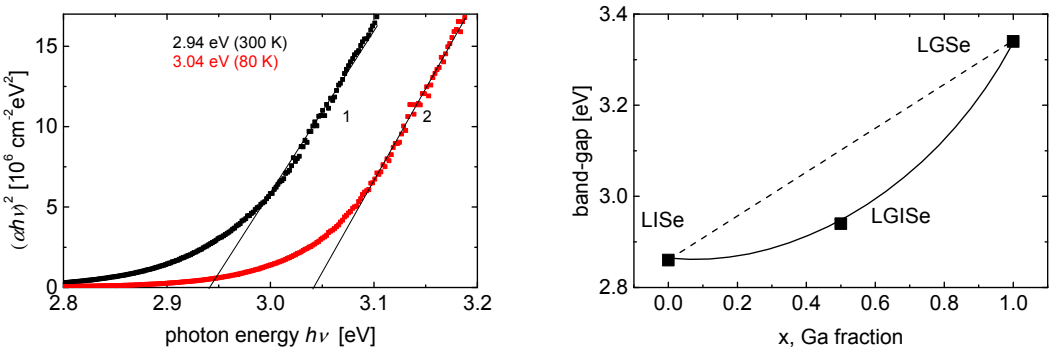

(**a**) (**b**)

Figure 4. (**a**) Fundamental absorption edge for a 60-μm-thick LGISe plate, represented as $(\alpha h\nu)^2 = f(h\nu)$, at T = 300 K (1) and 80 K (2); (**b**) Band-gap values for $LiInSe_2$ (LISe), $LiGaSe_2$ (LGSe), and LGISe, derived from room-temperature absorption measurements.

Photoluminescence (PL) spectra were recorded at 300 and 80 K using a diffraction luminescence spectrometer SDL1 (LOMO JSC, St. Petersburg, Russia) and a cooled FEU-83 photomultiplier (Ekran Optical Systems, Novosibirsk, Russia). By means of an MDR2 monochromator (LOMO JSC, St. Petersburg, Russia), different spectral ranges were selected from the 1 kW Xe lamp spectrum to excite PL in LGISe. Typical PL spectra recorded at 80 K for excitation with 3.1, 2.75 and 2.48 eV photon energy (400, 450 and 500 nm, respectively) are shown in Figure 5. Emission occurs basically in two spectral ranges: 1.5 to 2.0 eV and 1.1 to 1.4 eV.

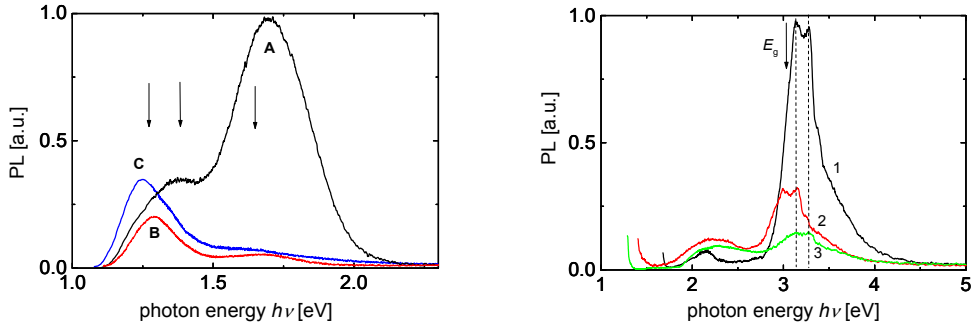

(**a**) (**b**)

Figure 5. (**a**) PL spectra recorded with $LiGa_{0.5}In_{0.5}Se_2$ crystals at 80 K for excitation at 3.1 eV (400 nm, curve A), 2.75 eV (450 nm, B), and 2.48 eV (500 nm, C). The arrows in (**a**) indicate the photon energies ($h\nu$ = 1.265, 1.38, and 1.65 eV) for which the photoluminescence excitation (PLE) spectra were measured; (**b**) 80 K PLE spectra of $LiGa_{0.5}In_{0.5}Se_2$ recorded for emission at 1.65 eV (750 nm, curve 1), 1.38 eV (900 nm, 2), and 1.265 eV (980 nm, 3). The arrow in (b) indicates the band-gap E_g at 80 K.

Table 4. Results from a Gaussian deconvolution analysis of the PL spectra of $LiGa_{0.5}In_{0.5}Se_2$.

#	Position of Peak Maximum		FWHM
	eV	nm	eV
1	1.247	994	0.164
2	1.291	960	0.187
3	1.350	918	0.247
4	1.702	728	0.329

The results from a Gaussian deconvolution analysis of the PL spectra yielding four components are summarized in Table 4: they include the peak positions in photon energies (eV) and wavelengths (nm)

as well as the full width at half-maximum (FWHM). Spectrum A recorded for 3.1 eV excitation consists of components 4, 3, 2 from Table 4, whereas spectra B and C are constituted mainly by components 2 and 1, respectively. The PL intensity is rather low at room temperature but it increases by two orders of magnitude as the crystal is cooled down to 80 K. Similar PL emission with a main peak near 1.8 eV has been observed in LISe [16] and LGSe. Another PL band was observed in LISe near 2.4 eV [16]: both bands, at 1.8 and 2.4 eV, were associated with a radiative recombination in donor-acceptor pairs (DAPs) [16]. Photoluminescence excitation (PLE) spectra recorded at different photon energies are shown in Figure 4b. One can see that the dominating red PL is excited most effectively in a group of narrow bands at 2.998, 3.147 and 3.275 eV (413, 394 and 378 nm, respectively). The arrow in Figure 4b marks the band-gap value of 3.04 eV for LGISe derived from the low-temperature absorption measurements. Thus, the main band near 3.2 eV in the PLE spectra of LGISe agrees well with the band-gap value and corresponds to band-to-band electronic transitions. There are no other appreciable bands in the PLE spectra for 1.7 eV emission in LGISe and this agrees with the model of DAP recombination [16]. DAP recombination takes place following band-to-band transitions when free charge carriers of different sign (electrons and holes) are generated. Subsequently these free electrons and holes are captured by traps and stay there for a long time at low temperature. At a later stage, there may be a radiative recombination between such captured charge carriers (donors and acceptors) [16]. The low energy group of PL bands near 1.25 eV is observed not only by band-to-band excitation but also by excitation in a broad band near 2.2 eV (Figure 4b, curves 2, 3). This is an indication of an intracenter PL mechanism while the 2.2 eV signal corresponds to an absorption band of some point defect (presumably a cation antisite defect). The variety of PL emission and the fine structure of the PLE spectra near 3.2 eV may be a result of several nonequivalent positions of the Li^+ ions in LGISe.

4. Dispersion, Birefringence and Nonlinearity

Two semiprisms (inset Figure 6a), with a reflecting face parallel to a principal plane, were prepared from LGISe (yellow color) for measurement of the three principal refractive indices by the autocollimation method. The three refractive indices were measured by the autocollimation method at 23 wavelengths between 0.48 and 12 μm [13]. The data were fitted by one-pole Sellmeier equations with quadratic IR correction term. The Sellmeier coefficients are summarized in Table 5. Figure 6a shows the measured refractive index values and the calculated curves using the fitted Sellmeier equations. Interestingly, n_y and n_z of LGISe exceed, in a substantial part of the mid-IR transmission range, the corresponding values for LISe (which in turn are larger than those for LGSe).

Table 5. Sellmeier equations for LGISe, $n^2 = A + B/(\lambda^2 - C) - D\lambda^2$, where λ is in μm, valid in the 0.48–12 μm range.

n	*A*	*B*	*C*	*D*
n_x	5.03847	0.18748	0.07033	0.00204
n_y	5.24012	0.21386	0.07033	0.00193
n_z	5.26219	0.21331	0.07550	0.00209

The Sellmeier equations predict index crossing of n_y and n_z near the cut-off edges. However, in the major part of the transmission window the correspondence between the dielectric and crystallographic axes in the orthorhombic LGISe is *xyz* = *bac* and this relationship can be adopted for reporting the phase-matching angles (defined in the *xyz* frame) and the nonlinear coefficients (defined in the *abc* frame). This means that the two optic axes which determine the propagation directions where the index of refraction is independent of polarization move from the *x*–*z* principal plane (in the major part of the clear transmission) to the *x*–*y* plane (towards the edges). The angle V_z between the two optic axis and the *z*-principal axis, is determined by $sinV_Z = \frac{n_Z(n_Y^2 - n_X^2)^{1/2}}{n_Y(n_Z^2 - n_X^2)^{1/2}}$. It approaches 90° towards the crossing points where absorption is already substantial but in the interesting for practical applications clear transmission range the angle V_z is almost constant, around 75°. Thus the optically negative ($V_z > 45°$)

biaxial LGISe crystal can be regarded as quasi-uniaxial, which is a consequence of the fact that the two indices n_y and n_z are very close. Therefore no phase-matching can be expected for propagation directions in the vicinity of the x-principal axis.

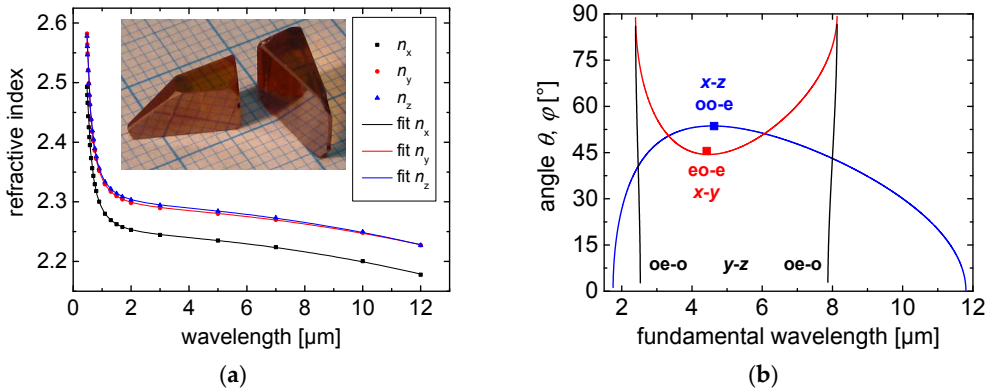

(**a**) (**b**)

Figure 6. (**a**) Measured refractive indices of LGISe (symbols) and calculated curves using the Sellmeier coefficients from Table 5 (the inset shows the semiprisms fabricated for the measurements); and (**b**) Second harmonic generation (SHG) phase-matching curves in the three principal planes of LGISe. The symbols correspond to experimental SHG points at 4.63 µm in the x–z plane and at 4.42 µm in the x–y principal plane.

This can be seen from the second harmonic generation (SHG) phase-matching curves calculated which are presented in Figure 6b. The predicted phase-matching angles agree very well with the SHG measurements performed in the x–y and x–z planes with femtosecond pulses. In the x–z plane the deviation at 4.63 µm was within the cut accuracy while in the x–y plane, at a fundamental wavelength of 4.42 µm, the internal experimental phase-matching angle was roughly 1° larger than the calculated one. The SHG range for the fundamental wavelength, covered by interactions in the principal planes that possess non-vanishing effective nonlinearity d_{eff}, extends from 1.75 to 11.8 µm.

Phase-matching calculations for general type three-wave interactions in the x–y and x–z planes, where broad tuning can be realized for optical parametric generators, amplifiers and oscillators were presented in [13]. As already mentioned, similar to the two parent compounds LISe and LGSe, LGISe will not suffer from TPA at a pump wavelength of 1.064 µm and phase matching for such down-conversion nonlinear processes is feasible in the x–y and x–z principal planes.

In the principal planes, the expressions for the effective nonlinearity d_{eff} of LGISe read:

$$d_{eff}^{eoe} = d_{eff}^{oee} = -(d_{24}\sin^2\phi + d_{15}\cos^2\phi) \quad (x-y \text{ plane}) \tag{1a}$$

$$d_{eff}^{oeo} = d_{eff}^{eoo} = -d_{24}\sin\theta \quad (y-z \text{ plane}) \tag{1b}$$

$$d_{eff}^{ooe} = d_{31}\sin\theta \quad (x-z \text{ plane}, \theta < V_z) \tag{1c}$$

with superscripts "o" and "e" denoting the ordinary and extraordinary beams. LGISe behaves as an optically negative uniaxial crystal in the x–y and x–z (for $\theta < V_z$) planes, and as an optically positive uniaxial crystal in the y–z plane. Under Kleinman symmetry, $d_{15} = d_{31}$ is satisfied.

The elements d_{il} of the nonlinear tensor have been investigated by SHG using type-I or type-II interactions in the principal planes of LGISe. Since femtosecond pulses were applied, the use of very thin oriented LGISe and reference samples (LISe and LGSe) makes it possible to neglect the effects of absorption, beam walk-off, and focusing with the data analysis in the low-depletion limit derived from standard plane-wave SHG theory. The conversion efficiency was kept low, and we corrected the relative measurements only for the crystal thickness and the slightly different index of refraction and Fresnel reflections. Unfortunately, only for type-I interaction, the spectral acceptance of all three samples was much larger than the spectral bandwidth of the femtosecond pulses near 4.6 µm.

The femtosecond source at 1 kHz repetition rate was a $KNbO_3$-based optical parametric amplifier. The single pulse energy was in the 2–3 μJ range. The measurements were performed simultaneously with the two reference (LISe and LGSe) samples.

The coefficient d_{31} was estimated by type-I SHG in the x–z plane from Equation (1c). The LGISe sample for SHG in the x–z plane was cut at θ = 53.6° and had a thickness of 0.7 mm. The reference LGSe (0.9 mm thick) and LISe (0.86 mm thick) samples were cut at θ = 56.4° and θ = 46.7°, respectively. We obtained d_{31}(LGISe) = 0.94d_{31}(LISe) and d_{31}(LGISe) = 1.03d_{31}(LGSe). The ratio of the nonlinear coefficients of LISe and LGSe was 1.1, close to the ratio of 1.19 estimated at 2.3 μm from previous measurements [2,6]. Thus, it can be concluded that within the experimental accuracy, ±10% in the relative measurements, LGISe has nonlinearities of the same order of magnitude as the other two selenide compounds. While similar measurements were also performed for type-II SHG in the x–y plane to determine d_{24} from Equation (1a), the thickness of the samples did not permit reliable estimation because the spectral acceptance was not sufficient in order to consider samples of different thickness unaffected by this factor.

5. Conclusion

LGISe, a new quaternary nonlinear crystal for the mid-IR grown as a solid-solution in the system of the two ternary lithium selenides LGSe and LISe, exhibits the same orthorhombic structure (*mm2*) as the parent compounds but is more technological with regard to the growth process since its homogeneity range is broader in the phase diagram. It is transparent between 0.47 and 13 μm with a band-gap of 2.94 eV at room temperature. The Sellmeier equations, constructed on the basis of refractive index measurements, reproduce well SHG phase-matching angles in the principal dielectric planes. The fundamental wavelength range for the SHG process extends from 1.75 to 11.8 μm. The second-order nonlinearity of LGISe has an intermediate value, between those of LGSe and LISe. Since the band-gap of LGISe is much closer to that of LISe, the electrical conductivity and response to thermal neutrons are expected to be also similar. Additional gain in efficiency for thermal neutron detection is expected due to substitution of half of the ^{115}In ions by Ga and the resulting weakening of the competing interaction mechanism with the neutrons. Intense DAP luminescence allows one to use LGISe also as a scintillator for detection of thermal neutrons.

Acknowledgments: We thank Sergey F. Solodovnikov for the X-ray structural analysis and Vladimir L. Panyutin for the useful discussions and his help in the SHG experiments and in the preparation of this manuscript. This work was supported by the Russian Foundation of Basic Research (Grant No. 15-02-03408a).

Author Contributions: Ludmila Isaenko and Alexander Yelisseyev conceived and realized the structural studies, the transmission and photoluminescence measurements; Sergei Lobanov and Pavel Krinitsyn grew the crystals, Vitaliy Vedenyapin performed the refractive index measurements and analyzed the phase-matching; Valentin Petrov studied the SHG and determined the nonlinear coefficients; Ludmila Isaenko, Alexander Yelisseyev and Valentin Petrov wrote the paper.

Conflicts of Interest: The authors declare no conflict of interest. The founding sponsors had no role in the design of the study; in the collection, analyses, or interpretation of data; in the writing of the manuscript, and in the decision to publish the results.

Abbreviations

The following abbreviations are used in this manuscript:

LGSe	$LiGaSe_2$
LISe	$LiInSe_2$
LGISe	$LiGa_{0.5}In_{0.5}Se_2$
TPA	two-photon absorption
PL	photoluminescence
PLE	photoluminescence excitation
FWHM	full width at half-maximum
DAP	donor-acceptor pair
SHG	second harmonic generation

References

1. Isaenko, L.; Yelisseyev, A.; Lobanov, S.; Titov, A.; Petrov, V.; Zondy, J.-J.; Krinitsin, P.; Merkulov, A.; Vedenyapin, V.; Smirnova, J. Growth and properties of $LiGaX_2$ (X = S, Se, Te) single crystals for nonlinear optical applications in the mid-IR. *Cryst. Res. Technol.* **2003**, *38*, 379–387. [CrossRef]
2. Petrov, V.; Yelisseyev, A.; Isaenko, L.; Lobanov, S.; Titov, A.; Zondy, J.-J. Second harmonic generation and optical parametric amplification in the mid-IR with orthorhombic biaxial crystals $LiGaS_2$ and $LiGaSe_2$. *Appl. Phys. B* **2004**, *78*, 543–546. [CrossRef]
3. Isaenko, L.; Vasilyeva, L.; Merkulov, A.; Yelisseyev, A.; Lobanov, S. Growth of new nonlinear crystals $LiMX_2$ (M = Al, In, Ga; X = S, Se, Te) for the mid-IR optics. *J. Cryst. Growth* **2005**, *275*, 217–223. [CrossRef]
4. Isaenko, L.; Yelisseyev, A.; Lobanov, S.; Krinitsin, P.; Petrov, V.; Zondy, J.-J. Ternary chalcogenides $LiBC_2$ (B = In, Ga; C = S, Se, Te) for mid-IR nonlinear optics. *J. Non-Cryst. Sol.* **2006**, *352*, 2439–2443. [CrossRef]
5. Zondy, J.-J.; Petrov, V.; Yelisseyev, A.; Isaenko, L.; Lobanov, S. Orthorhombic crystals of lithium thioindate and selenoindate for nonlinear optics in the mid-IR. In *Mid-Infrared Coherent Sources and Applications*; Ebrahim-Zadeh, M., Sorokina, I., Eds.; Springer: Dordrecht, The Netherlands, 2008; pp. 67–104.
6. Fossier, S.; Salaün, S.; Mangin, J.; Bidault, O.; Thenot, I.; Zondy, J.-J.; Chen, W.; Rotermund, F.; Petrov, V.; Petrov, P.; et al. Optical, vibrational, thermal, electrical, damage and phase-matching properties of lithium thioindate. *J. Opt. Soc. Am. B* **2004**, *21*, 1981–2007. [CrossRef]
7. Petrov, V.; Zondy, J.-J.; Bidault, O.; Isaenko, L.; Vedenyapin, V.; Yelisseyev, A.; Chen, W.; Tyazhev, A.; Lobanov, S.; Marchev, G.; et al. Optical, thermal, electrical, damage, and phase-matching properties of lithium selenoindate. *J. Opt. Soc. Am. B* **2010**, *27*, 1902–1927. [CrossRef]
8. Petrov, V. Frequency down-conversion of solid-state laser sources to the mid-infrared spectral range using non-oxide nonlinear crystals. *Progress Quantum Electron.* **2015**, *42*, 1–106. [CrossRef]
9. Schunemann, P.G.; Setzler, S.D.; Pollak, T.M. Phase-matched crystal growth of $AgGaSe_2$ and $AgGa_{1-x}In_xSe_2$. *J. Cryst. Growth* **2000**, *211*, 257–264. [CrossRef]
10. Badikov, V.V.; Kuz'micheva, G.M.; Panyutin, V.L.; Rybakov, V.B.; Chizhikov, V.I.; Shevyrdyaeva, G.S.; Shcherbakov, S.I. Preparation and structure of $AgGa_{1-x}In_xSe_2$ single crystals. *Inorg. Mater.* **2003**, *39*, 1028–1034. [CrossRef]
11. Badikov, V.V.; Laptev, V.B.; Panyutin, V.L.; Ryabov, E.A.; Shevyrdyaeva, G.S. Study of nonlinear-optical characteristics of $AgGa_{1-x}In_xSe_2$ crystals. *Quantum Electron.* **2005**, *35*, 252–256. [CrossRef]
12. Andreev, Y.M.; Atuchin, V.V.; Lanskii, G.V.; Pervukhina, N.V.; Popov, V.V.; Trocenko, N.C. Linear optical properties of $LiIn(S_{1-x}Se_x)_2$ crystals and tuning of phase matching conditions. *Sol. State Sci.* **2005**, *7*, 1188–1193. [CrossRef]
13. Vedenyapin, V.; Isaenko, L.; Yelisseyev, A.; Lobanov, S.; Tyazhev, A.; Marchev, G.; Petrov, V. New mixed $LiGa_{0.5}In_{0.5}Se_2$ nonlinear crystal for the mid-IR. *Proc. SPIE* **2011**, *7917*. [CrossRef]
14. Tupitsyn, E.; Bhattacharya, P.; Rowe, E.; Matei, L.; Groza, M.; Wiggins, B.; Burger, A.; Stowe, A. Single crystal of $LiInSe_2$ semiconductor for neutron detector. *Appl. Phys. Lett.* **2012**, *101*. [CrossRef]
15. Wiggins, B.; Groza, M.; Tupitsyn, E.; Lukosi, E.; Stassun, K.; Burger, A.; Stowe, A. Scintillation properties of semiconducting $^6LiInSe_2$ crystals to ionizing radiation. *Nucl. Instr. Meth. Phys. Res. A* **2015**, *801*, 73–77. [CrossRef]
16. Cui, Y.; Bhattacharya, P.; Buliga, V.; Tupitsyn, E.; Rowe, E.; Wiggins, B.; Johnstone, D.; Stowe, A.; Burger, A. Defects in $^6LiInSe_2$ neutron detector investigated by photo-induced current transient spectroscopy and photoluminescence. *Appl. Phys. Lett.* **2013**, *103*, 092104. [CrossRef]
17. Wiggins, B.; Bell, J.; Burger, A.; Stassun, K.; Stowe, A.C. Investigations of $^6LiIn_{1-x}Ga_xSe_2$ semi-insulating crystals for neutron detection. *Proc. SPIE* **2015**, *9593*. [CrossRef]
18. Isaenko, L.I.; Vasilyeva, I.G. Nonlinear $Li^{III}C^{VI}_2$ crystals for mid-IR and far-IR: Novel aspects in crystal growth. *J. Cryst. Growth* **2008**, *310*, 1954–1960. [CrossRef]